Optimization of Temperature Uniformity in Sensible and Latent Heat Large Packed-Bed Thermal Energy Storage Systems Using Molten Salt

Nayoung Kim^a, Taeho Roh^a Jeong Ik Lee^{a*}
^aDepartment of Nuclear and Quantum Engineering Korea Advanced Institute of Science and Technology
*Corresponding author: jeongiklee@kaist.ac.kr

*Keywords: Packed bed thermal energy storage, Sensible heat, Latent heat, Aspect ratio optimization

1. Introduction

The growing demand for high-temperature heat in the power and industrial sectors underscores the need for gigawatt-hour (GWh)-scale thermal energy storage (TES) systems capable of multi-hour load shifting [1–3]. Such systems support renewable integration and enable coupled operation with advanced nuclear reactors, particularly in hybrid energy systems requiring flexible load-following capability. In the nuclear context, advanced reactors such as high-temperature gas-cooled reactors (HTGRs), molten salt reactors (MSRs), and small modular reactors (SMRs) are increasingly emphasized as promising heat sources for both electricity generation and industrial process heat. Their high outlet temperatures and stable baseload operation make them well-suited for integration with large-scale TES, thereby enhancing flexibility and reliability. Molten salts are recognized as suitable storage media due to their high volumetric heat capacity, thermal and chemical stability, and cost competitiveness. Solar salt (NaNO3-KNO3) has been widely demonstrated in concentrating solar power (CSP) plants [4] and adopted in the Natrium reactor demonstration project [5], confirming its relevance for nuclear-TES integration. Conventional molten salt TES relies on the two-tank configuration, where hot and cold tanks allow reliable charge-discharge operation. However, at capacities above several hundred megawatthours, tank scaling leads to exponential increases in structural requirements, land use, and capital costs, along with complex piping networks and maintenance demands [6,7]. To overcome these challenges, packedbed TES (PBTES) has been proposed as a single-tank alternative. By directly contacting molten salt with a solid filler, PBTES offers simpler construction, reduced cost, enhanced heat transfer area, reduced stratification, and potential capital cost reductions of over 30% compared with two-tank systems [8,9].

PBTES can be categorized into sensible heat (SH) and latent heat (LH) approaches. SH storage, extensively studied since the early 20th century [10], benefits from operational simplicity and stability but suffers from low energy density, resulting in large tank volumes. LH storage, based on encapsulated phase change materials (PCMs), provides higher energy density and nearisothermal discharge profiles [11–13]. Despite advances in encapsulation, challenges remain in thermal conductivity enhancement, capsule durability, void

fraction control, and scalability to GWh-scale applications.

This study investigates large-scale PBTES systems operating in the 550-310 °C range with solar salt as the storage medium. A capacity of 1000 MWhth is selected to reflect multi-hour applications, which also corresponds to the scale required for coupling with SMRs and advanced reactors delivering several hundred megawatts of thermal power. To clearly isolate geometric effects, variations in flow velocity and tank diameter are intentionally excluded. The comparative performance of sensible heat (SH) and latent heat (LH) configurations is therefore evaluated with a focus on discharge temperature uniformity and aspect ratio (AR) optimization, emphasizing their influence on thermal front behavior using the GAMMA+ code developed by KAERI. By defining this scope, the study establishes practical design criteria for ensuring uniform thermal response in both sensible and latent heat packed-bed TES systems.

2. Methods and Results

The overall design and operating conditions of the packed bed thermal energy storage (PBTES) system are summarized in Table 2 and Table 3. To ensure a fair comparison, both sensible heat (SH) and latent heat (LH) configurations were analyzed under identical boundary conditions, including the total storage capacity, discharge duration, operating temperature window (550–310 °C), bed porosity, particle size, and geometric parameters.

$$Q_{SH} = (1 - \varepsilon)\rho_s c_{p,s} (T_{hot} - T_{cold}) V_{bed}$$
 (1)

$$Q_{LH} = \frac{\phi_{PCM}\rho_{PCM}q_{eff} + (1 - \varepsilon) \left[\phi_{shell}\rho_{shell}c_{p,shell}(T_{hot} - T_{cold})\right]V_{bed}}{\left[\phi_{shell}\rho_{shell}c_{p,shell}(T_{hot} - T_{cold})\right]}V_{bed}$$

$$q_{eff} = L + c_{p,l}(T_{hot} - T_m) + c_{p,s}(T_m - T_{cold})$$
 (3)

where ϵ = porosity, L = latent heat, $c_{p,l}$, $c_{p,s}$ = specific heat of PCM (liquid, solid), T_{hot} , T_{cold} , T_m = hot, cold, and melting temperatures, ϕ =volume fraction, V_{bed} = packed bed volume. And Subscript s = solid sensible medium (concrete), PCM = phase change material, shell = capsule shell

In Equations (1)– (3), Q_{SH} denotes the total sensible heat storage capacity of the packed bed, determined from

the solid filler properties, bed porosity, and the hot–cold temperature difference. Q_{LH} represents the total latent heat storage capacity of the encapsulated PCM bed, including both the phase change contribution of the PCM and the sensible heat of the capsule shell. q_{eff} is the effective heat storage per unit PCM mass, defined as the sum of the latent heat of fusion and the sensible heat contributions above and below the melting temperature.

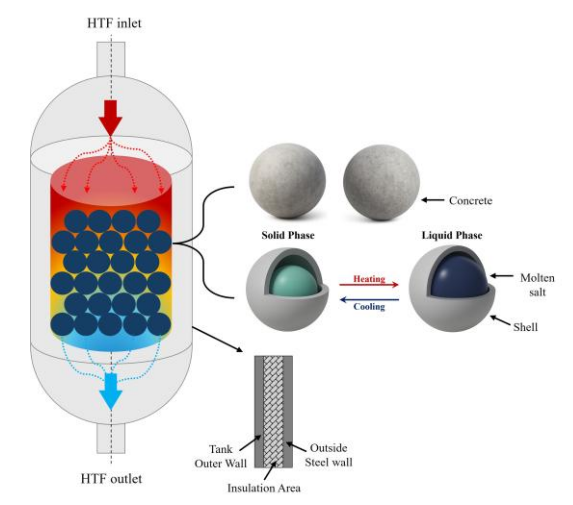


Fig. 1 Overall diagram of packed-bed TES with concrete (SH) and encapsulated PCM (LH)

2.1 Material selection

Material selection was carried out according to three main criteria: (i) thermal and chemical stability within the defined operating range, (ii) compatibility and resistance against corrosion, and (iii) cost and manufacturability. For SH storage, concrete was chosen. Although SH media inherently result in lower volumetric energy density and thus significantly larger tank sizes compared with LH systems as illustrated in Fig. 2, concrete remains an attractive choice due to its low cost, wide availability, ease of casting into complex geometries, and robust thermal cycling performance.

For LH storage, the melting point criterion $310 + \Delta T$ $< T_{\rm m} < 550 - \Delta T$ was applied to ensure safe operation within the defined window. Candidate materials considered included carbonate and chloride eutectics, as summarized in Table 1. These salts exhibit melting points in the range of 380-500 °C and latent heats of 240-380 kJ/kg. While they provide high storage density, their low thermal conductivity necessitates additional design measures such as graphite matrices, metal foams, or microencapsulation. Chloride salts offer favorable thermal capacity but are hygroscopic and corrosionprone, requiring strict material compatibility measures. Carbonates are relatively more stable in CO2 environments. Metallic PCMs such as Zn have excellent thermal conductivity but increase system mass and impose strict requirements on container compatibility.

Table 1. LH PCM Candidates within the Design Operating Temperature Range (310–550°C)

Operating rem	perature Range (510–5	30 C)
Family	Material	T _m (°C)

	Na ₂ CO ₃ -Li ₂ CO ₃		
Carbonate	(48:52)	~500	
Chloride	NaCl–MgCl ₂ (eutectic)	440-450	
Chloride	KCl-MgCl ₂ (eutectic)	420-430	

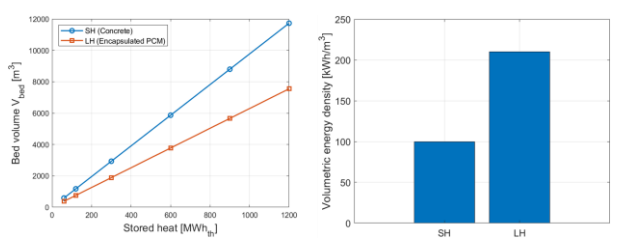


Fig. 2 Bed volume vs. Stored heat for SH and LH TES (left) Volumetric energy density comparison of SH and LH TES (right)

Table 2. Common Operating Condition (Target)

Parameters	Value	Unit		
Total Stored heat	1000	MWh _{th}		
Discharging time	6	hour		
Operating temperature	550°C - 310	°C		
Heat transfer fluid	Solar salt	-		

Table 3. Design Geometry Parameters Condition

Parameters	Value	Unit
Porosity of bed	0.36	ı
Particle diameter	3	mm
Capsule metallic shell thickness	2	mm
Capsule internal diameter	3	cm
Capsule void	20	%

Table 4. Thermal properties of Material in Packed bed

Parameters	Value	Unit	
SH Storage medium	Concrete		
Density	2067	kg/m ³	
Specific heat capacity	1.16	kJ/kgK	
Thermal conductivity	2.0	W/mK	
LH Storage medium	Na ₂ CO ₃ -Li ₂ CO ₃ (48:52)		
Melting point	500	°C	
Latent heat	370	kJ/kg	
Density	2320	kg/m ³	
Specific heat capacity (liquid)	1.7	kJ/kgK	
Specific heat capacity (solid)	1.5	kJ/kgK	
Thermal conductivity	0.6	W/mK	
LH Capsule metallic shell	Al_2O_3		
Density	3900	kg/m ³	
Specific heat capacity	0.88	kJ/kgK	
Thermal conductivity	20	W/mK	

2.2 Validation results

The performance of the GAMMA+ model for packedbed thermal energy storage was validated against two experimental cases. For sensible heat storage, simulation results were compared with the Sandia pilot-scale thermocline experiment [14] using a 6.1 m tall, 3.0 m diameter tank packed with quartzite rock and sand and operated with Solar Salt. Axial temperature profiles during discharge showed good agreement with the model, with mean absolute percentage errors (MAPE) ranging from 0.67 % to 8.96 %. MAPE, which represents the average relative deviation between experimental and simulated temperatures, is generally considered to indicate strong agreement when below 10 %. In this study, errors remained below 2 % during the early discharge period, while the temporary rise to 8.96 % at 1.5 h was associated with sharp thermal gradients near the moving thermocline, and still within acceptable bounds. For latent heat storage, validation was conducted against the capsule-based experiment by Bellan et al. [15], in which air was used as the heat transfer fluid. Capsule temperatures at two radial positions matched experimental values within ±2 °C during both charging and discharging. The onset and duration of the phase change plateau were predicted within 3-4 % of the measurements, confirming that the model accurately captured latent heat absorption and release dynamics. As summarized in Fig. 3, both SH and LH cases demonstrate that GAMMA+ reliably reproduces thermocline propagation and phase change behavior, supporting its suitability for the design and optimization of large-scale TES systems.

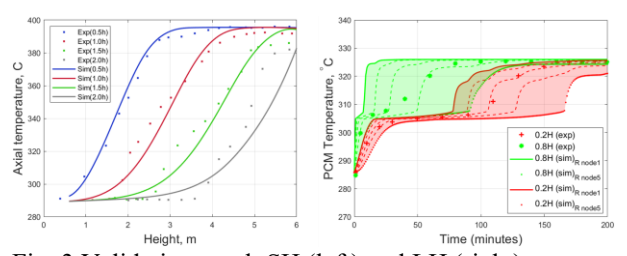


Fig. 3 Validation result SH (left) and LH (right)

2.3 Aspect ratio Optimization

The GAMMA+ simulations were performed under the boundary conditions in Tables 1–3 to investigate the impact of aspect ratio (AR = H/D) on thermal behavior. Both SH and LH systems were modeled with experimentally based thermophysical properties. For LH storage, the metallic capsule shell and temperature-dependent PCM properties were explicitly included to account for added thermal resistance and phase-change buffering. Geometric irregularities were excluded so that the effect of AR could be isolated.

AR optimization was defined by minimizing outlet temperature non-uniformity, quantified as the root-mean-squared deviation (RMSD) across radial nodes:

$$RMSD = \sqrt{\frac{1}{N} \sum_{i=1}^{N} (T_i - \bar{T})^2}$$
 (4)

where T_i are nodal outlet temperatures and \overline{T} is their average. RMSD is adopted instead of mean deviation because it penalizes larger local deviations and remains independent of node count.

Table 5 summarizes RMSD values for AR = 1–5. For SH TES, RMSD decreased from 56.1 °C at AR = 1 to <0.05 °C at AR \geq 3. For LH TES, RMSD exceeded 60 °C at AR = 1–2, converging to <0.2 °C only for AR \geq 4. These results yield minimum recommended AR values of 3 (SH) and 4 (LH).

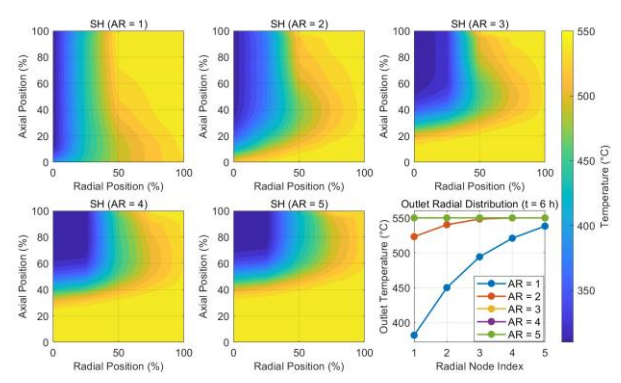


Fig. 4 Temperature fields of SH TES for different aspect ratios (AR=1-5) and corresponding outlet radial temperature distributions at t=6h

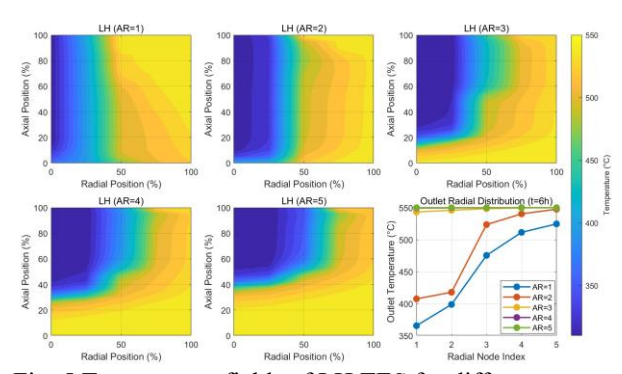


Fig. 5 Temperature fields of LH TES for different aspect ratios (AR=1-5) and corresponding outlet radial temperature distributions at t=6h

Table 5 Table 5. RMSD outlet temperature of SH and LH TES for AR = 1-5

Type	AR=1	AR=2	AR=3	AR=4	AR=5
SH	56.098	10.239	0.046	0.002	0.001
LH	62.635	61.577	2.510	0.193	0.039

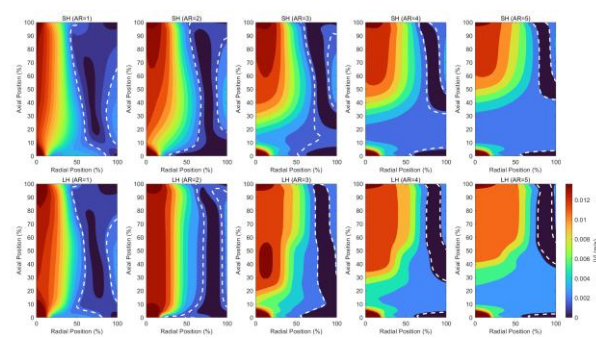


Fig. 6 Velocity distributions of SH (top) and LH (bottom) TES at AR = 1-5. White dashed lines indicate stagnation regions (dead zones)

Fig. 4 and Fig. 5 provide further insight into these results. In SH TES, low AR cases exhibited strong radial gradients and tilted thermal fronts due to pronounced flow maldistribution, while $AR \geq 3$ produced nearly parallel fronts consistent with plug-flow behavior. In LH TES, larger deviations persisted at AR = 1-2 because the metallic shell enclosing each PCM capsule introduced additional thermal resistance and local conduction delays. Nevertheless, the latent heat buffering effect attenuated temperature gradients, leading to thermal fronts that appeared flatter than in SH TES despite wider stagnation regions.

Fig. 6 highlights the importance of stagnation zones in low-velocity TES operation. Here, stagnation was defined as regions with velocity magnitude below 0.002 m/s. In SH TES, AR = 1-2 produced extensive stagnation near the walls and bottom, which directly translated into distorted thermal fronts and outlet nonuniformity. At AR \geq 3, these stagnation zones diminished, and the flow spread more evenly across the cross-section, reducing RMSD accordingly. In LH TES, capsule-induced resistance preserved broader stagnation zones even at AR = 3, delaying uniformity until $AR \ge 4$. However, the latent heat absorption/release buffered this maldistribution, partially flow decoupling uniformity from the thermal response.

Together, these results confirm that SH TES achieves acceptable uniformity with AR ≥ 3 , while LH TES requires AR ≥ 4 to overcome capsule-related resistance. This emphasizes that optimization under low-velocity conditions must account for both hydrodynamic and thermal mechanisms: stagnation zone suppression on one hand, and phase-change buffering on the other. Moreover, while LH TES demands a larger AR, it offers superior volumetric energy density, highlighting a tradeoff between geometric compactness and storage efficiency.

3. Summary and Conclusion

This study investigated the optimization of temperature uniformity in large packed-bed thermal energy storage (TES) systems employing sensible heat (SH) and latent heat (LH) media with molten salt as the heat transfer fluid. The GAMMA+ code was used to simulate thermal and flow behavior under nuclear integration conditions, with thermophysical properties

derived from experimental data. For the LH case, the metallic capsule shell and the temperature-dependent properties of the phase change material (PCM) were explicitly modeled to account for additional thermal resistance and buffering during melting and solidification.

The aspect ratio (AR) was systematically varied, and outlet temperature non-uniformity was quantified using the root-mean-squared deviation (RMSD) across radial nodes. Results demonstrated that SH TES required AR \geq 3 to achieve RMSD < 0.05 °C, whereas LH TES required $AR \ge 4$ to suppress outlet non-uniformity. Flow-field analysis indicated that stagnation zones, defined as lowvelocity regions, were more pronounced at low AR. However, the contrast in uniformity between SH and LH TES was primarily governed by the intrinsic material characteristics. In SH TES, heat transfer through a continuous solid medium enabled uniform thermal fronts once AR ≥ 3. In LH TES, capsule shells imposed additional conduction resistance while the phase-change process induced local buffering, delaying uniformity even at higher AR.

In conclusion, the minimum recommended AR is 3 for SH TES and 4 for LH TES, based on the criterion of minimizing outlet temperature non-uniformity. SH TES offers greater compactness by achieving acceptable uniformity at lower AR, whereas LH TES provides superior volumetric energy density but requires larger AR due to its intrinsic material behavior. Rather than a simple trade-off, these results establish practical design criteria for selecting and scaling TES configurations in nuclear integration scenarios. At the 1000 MWh_{th} scale, the findings provide actionable guidance for ensuring multi-hour load shifting and stable coupled operation with small modular and next-generation reactors.

It is further noted that the present study focused solely on geometric effects, with flow velocity and tank diameter fixed. Future work should extend the analysis by incorporating these parameters to develop more generalized design guidelines for large-scale packed-bed TES systems.

ACKNOWLEDGEMENT

This work was supported by the National Research Foundation of Korea (NRF) grant funded by the Korea government (MSIT) (No. RS-2024-00457356).

REFERENCES

- [1] Zunft, S., Hänel, M., Lücke, R., Nowi, A., & Schmücker, M. Adiabatic compressed air energy storage for the grid integration of wind power. Applied Energy, 137, 576–581, 2015.
- [2] Steinmann, W.D. Thermal energy storage systems for electricity generation: Current status and future prospects. Journal of Energy Storage, 8, 25–36, 2016.
- [3] IEA. Energy Storage Tracking Report. International Energy Agency, 2023.

- [4] Bradshaw, R.W., & Siegel, N.P. Molten nitrate salts for solar thermal energy storage. Solar Energy Materials and Solar Cells, 21(2), 173–181, 2008.
- [5] TerraPower. Natrium reactor and integrated energy system. Project documentation, 2021–2023.
- [6] Gil, A., Medrano, M., Martorell, I., Lázaro, A., Dolado, P., Zalba, B., & Cabeza, L.F. State of the art on high-temperature thermal energy storage for power generation. Part 1—Concepts, materials and modellization. Renewable and Sustainable Energy Reviews, 14(1), 31–55, 2010.
- [7] Medrano, M., Gil, A., Martorell, I., Potau, X., & Cabeza, L.F. State of the art on high-temperature thermal energy storage for power generation. Part 2—Case studies. Renewable and Sustainable Energy Reviews, 14(1), 56–72, 2010.
- [8] Steinmann, W.D. Hybridization of sensible and latent heat storage for high temperature applications. Energy Procedia, 69, 951–960, 2015.
- [9] Laing, D., Steinmann, W.D., Tamme, R., & Crespo, M.J. Test results of concrete thermal energy storage for parabolic trough power plants. Journal of Solar Energy Engineering, 128(3), 220–226, 2006.
- [10] Schumann, T.E.W. Heat transfer: A liquid flowing through a porous prism. Journal of the Franklin Institute, 208(3), 405–416, 1929.
- [11] Farid, M.M., Khudhair, A.M., Razack, S.A.K., & Al-Hallaj, S. A review on phase change energy storage: materials and applications. Energy Conversion and Management, 45(9–10), 1597–1615, 2004.
- [12] Zalba, B., Marín, J.M., Cabeza, L.F., & Mehling, H. Review on thermal energy storage with phase change: Materials, heat transfer analysis and applications. Applied Thermal Engineering, 23(3), 251–283, 2003.
- [13] Cabeza, L.F., Castell, A., Barreneche, C., de Gracia, A., & Fernández, A.I. Recent progress in high temperature latent heat storage materials and systems: A review. Renewable and Sustainable Energy Reviews, 15(4), 1675–1695, 2011.
- [14] Pacheco, J. E., Showalter, S. K., & Kolb, W. J. (2002). Development of a molten-salt thermocline thermal storage system for parabolic trough plants. J. Sol. Energy Eng., 124(2), 153-159.
- [15] Bellan, S., Alam, T. E., González-Aguilar, J., Romero, M., Rahman, M. M., Goswami, D. Y., & Stefanakos, E. K. (2015). Numerical and experimental studies on heat transfer characteristics of thermal energy storage system packed with molten salt PCM capsules.